# Spin response and neutrino mean free path in neutron matter

**Luca Riz**

[1]Dipartimento di Fisica, University of Trento, via Sommarive 14, I–38123, Povo, Trento, Italy
[2]INFN-TIFPA, Trento Institute for Fundamental Physics and Applications, Trento, Italy

E-mail: `luca.riz@unitn.it`


**Stefano Gandolfi**

[3]Theoretical Division, Los Alamos National Laboratory, Los Alamos, NM

E-mail: `stefano@lanl.gov`


**Francesco Pederiva**

[1]Dipartimento di Fisica, University of Trento, via Sommarive 14, I–38123, Povo, Trento, Italy
[2]INFN-TIFPA, Trento Institute for Fundamental Physics and Applications, Trento, Italy

E-mail: `francesco.pederiva@unitn.it`

**Abstract.** The longitudinal and transverse density- and spin-density response functions in pure neutron matter (PNM) are derived over a wide range of densities within the Time Dependent Local Spin Density Approximation (TDLSDA). The underlying density functional was derived from an Auxiliary Field Diffusion Monte Carlo (AFDMC) computation of the equation of state of unpolarized and fully spin polarized pure neutron matter. In order to assess the dependence of the results on the specific underlying nucleon-nucleon Hamiltonian, we used both the phenomenological Argonne AV8′+UIX force, and local chiral forces up to next-to-next-to-leading-order (N$^2$LO). The resulting response function has then been applied to the study of the neutrino mean free path in PNM.

## 1. Introduction

As shown many years ago, the Weinberg-Salam Lagrangian [1] describing the interaction of neutrinos with baryonic matter can be translated, after a non relativistic reduction, into the calculation of a set of response functions to density and spin/isospin density operators [2]. Several non relativistic many-body calculations have been carried out over

time [3], in particular via a direct evaluation of the propagator in the context of the use of Skyrme-like forces [4, 5, 6], or by extending the Tamm-Dancoff approximation to the inclusion of dynamical correlations [7, 8, 9].

At present, computing response functions in a many-body system within an *ab-initio* scheme is technically possible, but still quite expensive from the computational point of view. In a previous paper [10] a fair compromise was devised between including the microphysics described by realistic nuclear potentials, that is usually addressable in ground state calculations, and a purely mean field treatment. This was achieved following the standard prescription suggested by the Hohenberg-Kohn theorem in order to obtain a realistic, though simplified, density functional, and employing it within the Time Dependent Local Density Approximation (TDLDA, see e.g. [11]). The first application was the study of the contribution of the longitudinal [10] isospin channel to the neutrino cross section in nuclear matter with an arbitrary value of the isospin asymmetry parameter. The TDLDA approximation has been also applied to the study of the transverse [12] isospin channel response functions for an arbitrary isospin asymmetry parameter.

In this paper we extend the TDLDA approach to the study of the density and spin-density response functions in pure neutron matter (PNM), both in the longitudinal and in the transverse channels. Since the functional used will depend on the density and magnetization of the neutron medium, the underlying ground state theory will be denoted as Local Spin Density Approximation (LSDA), and the dynamical version the Time Dependent Local Spin Density Approximation (TDLSDA). We do not limit our study to the unpolarized and fully-polarized cases, but we consider arbitrary spin polarization.

The key ingredient of any mean field calculation based on the Local Density Approximation (LDA) is an accurate density functional based on a pre-existing equation of state (EoS) $E[\rho]$. Following the Hohenberg-Kohn prescription, $E[\rho]$ can be extracted for a homogeneous system by simply fitting the exact energy as a function of the (spin/isospin-)density. By subtracting the energy of the free Fermi gas (FG) at the same density it is then possible to obtain the non-trivial part of the energy density functional. The LDA then allows to address problems for inhomogeneous systems and can be extended to study excited states.

In this paper we also want to check the robustness of the TDLSDA predictions against the underlying functional. In order to do that, we use two different Hamiltonians. The first includes a phenomenological two- plus three-neutron interaction (namely AV8′+UIX). The second employs modern local chiral effective field theory (EFT) potentials up to N²LO [13, 14, 15, 16, 17], and estimating the systematic error due to the uncertainty on the model potential.

The paper is organized as follows. In Sec. 2 we describe in some details the procedures and the results concerning the computation of the EoS for the Hamiltonians considered. In Sec. 3 we briefly review the formalism for computing the TDLSDA response function in both the longitudinal and transverse channels. Sec. 4 shows

the numerical results for the response functions, the neutrino mean free path and compressibility. Sec. 5 is devoted to conclusions. In App. Appendix A we present the calculation of the effective mass.

## 2. Equation of state

The first step in this analysis is the computation of the equation of state. This is achieved by means of Auxiliary Field Diffusion Monte Carlo Methods [18, 19]. As previously mentioned, two different nucleon-nucleon interaction schemes have been used. The first EoS (EOS-A thereafter) is derived from the well known Argonne AV8′ potential for the two-body interaction, plus the Urbana UIX interaction for the three body channel. This interaction has been widely used to study homogeneous neutron matter and nuclear matter properties (see [20, 21] and references therein). The second EoS (EOS$\chi$ thereafter) is based on potentials derived within chiral effective field theory ($\chi - EFT$). Among different implementations of the effective chiral potential which have been recently developed, we chose a local formulation up to N$^2$LO which have been derived by A. Gezerlis et al. [13, 14].

In Fig. 1 we report the results obtained from our calculations of fully spin polarized pure neutron matter (SPPNM) for densities ranging from $\rho_0/4$ up to $2\rho_0$, where $\rho_0 = 0.16$ fm$^{-3}$ is the nuclear saturation density. The results for pure neutron matter (PNM) are those obtained by Gandolfi et al. [22] and Tews et al. [16] for the phenomenological and the chiral interaction respectively. For the chiral potential we used the N$^2$LO(D2,E1) cutoff $R_0 = 1.0$ fm, $c_E = 0.62$ $c_D = 0.5$ as described in [15]. The specific choice of the operatorial parametrization is due to the fact that it provides an EoS close to that of AVX potentials. In addition, between the two cuftoffs presented in Ref. [15], the shorter cutoff value in coordinate space provides a stiffer EoS. This allows to analyze the sensitivity on the systematic uncertainties of the observables derived in the following analysis that includes somehow AVX case as a limiting case, maintaining a potential which gives realistic mass-radius relation for neutron stars. SPPNM energies were computed for N = 33 neutrons all with the same spin in a periodic box. We should remind that in QMC calculations the energy is projected starting from a state of given symmetry (in this case equivalent to a fully polarized liquid), and the projected values will not acquire components along orthogonal states. This, together with the constraints introduced to cope with the Fermion sign problem, provide the mechanism allowing for the simulation of the polarized phase, though this is not the ground state at any density. Similar calculation have been performed for the electron gas [23] and atomic $^3$He [24] several years ago. In order to reduce the impact of finite size effects, the potential was computed by a sum over the first neighbors of a given simulation cell. The statistical errors of the data reported in Fig. 1 are of the size of the symbols. The bands relative to the chiral potential results have been obtained using the prescription of Epelbaum et al. [25]. According to Ref. [25] the estimate of the theoretical error on an observable $X$
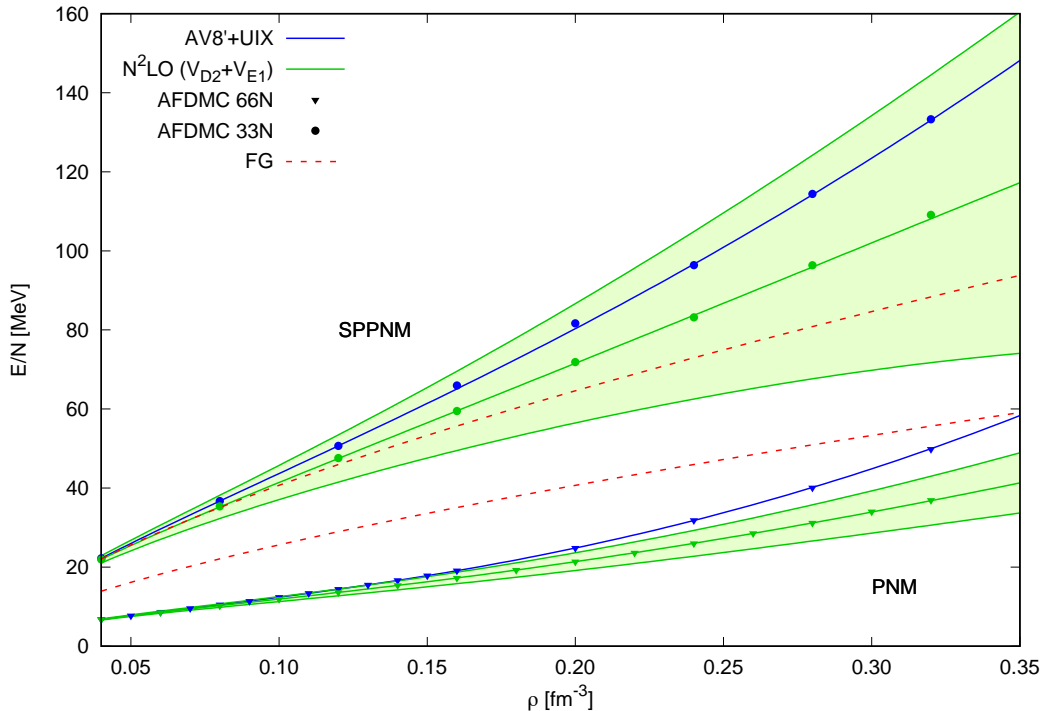
Figure 1: Equation of state for PNM (lower set) and for SPPNM (upper set) with AV8′+UIX (blue curves) and with chiral potential up to N²LO (green bands). More details on the potentials are described in the text. Errorbars for the chiral effective interaction have been computed according to Epelbaum et al. [25]. For the sake of comparison, we also report the corresponding curves for a free Fermi gas at the thermodynamic limit (red dotted curves).

is given by the following relation:

$$
\begin{aligned}
\Delta X^{\mathrm{NLO}} &= \max\left(Q^3 \times \left|X^{\mathrm{LO}}\right| \ , \ Q \times \left|X^{\mathrm{LO}} - X^{\mathrm{NLO}}\right|\right) \\
\Delta X^{\mathrm{N^2LO}} &= \max\left(Q^4 \times \left|X^{\mathrm{LO}}\right| \ , \ Q^2 \times \left|X^{\mathrm{LO}} - X^{\mathrm{NLO}}\right| \ , \right. \\
&\qquad \left. Q \times \left|X^{\mathrm{NLO}} - X^{\mathrm{N^2LO}}\right|\right) \ ,
\end{aligned}
\tag{1}
$$

where $Q = \max(p/\Lambda, m_\pi/\Lambda)$, with $\Lambda$ (normally $\simeq 1\,\mathrm{GeV}$) defining the breakdown scale, $m_\pi$ is the pion mass, and $p$ is the typical exchanged momentum. In addition there is a further constraint for theoretical uncertainties at NLO and N²LO, i.e. they must have at least the size of the actual higher order contribution. Higher order contributions are $Q^2 \times X^{\mathrm{LO}}$ and $Q^3 \times X^{\mathrm{NLO}}$ for the NLO and N²LO respectively. The latter is the dominant term. Instead of calculating the equation of state order by order we can estimate the theoretical error as $Q^3 \times X^{\mathrm{N^2LO}}$. This is an approximation, but it provides

a reasonable estimate (within $5 - 10\%$) compared to the full analysis. As an example we report in Fig. 2 the full analysis of the order by order expansion for the fully spin polarized case. We chose a breakdown scale $\Lambda = 600$ MeV (in accordance to Ref. [26] ) and we computed the typical exchanged momentum as:

$$p \sim \sqrt{2m\,\frac{3}{5}\frac{k_{\mathrm{F}}^{+^2}}{2m}}\,, \tag{2}$$

where $k_{\mathrm{F}}^{+}$ is the Fermi momentum of the polarized system at a given density and $m$ is the neutron mass. While at saturation density the theoretical uncertainties decrease, as predicted by the perturbative expansion, at $\rho = 2\rho_0$ the theoretical uncertainties remain of the same order between NLO and $N^2$LO. This signals that we are still within (though close to) the limit of applicability of the perturbative approach, and the chiral effective field theory is well-defined. The EoS for the polarized system and obtained
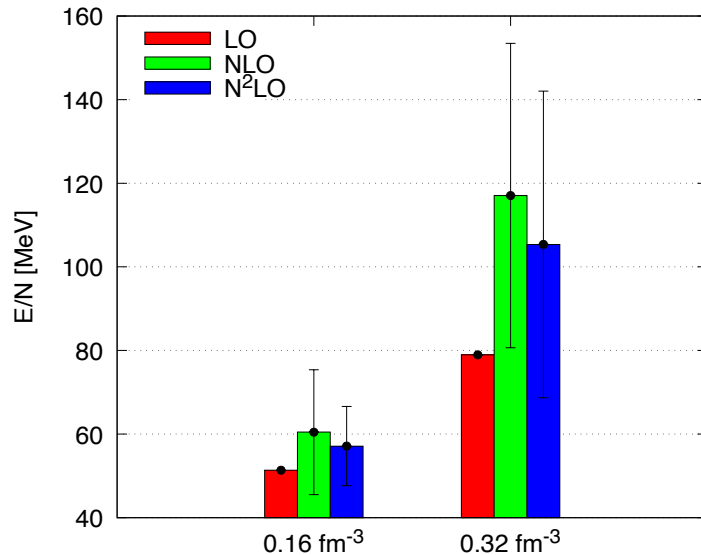


Figure 2: The histograms show the AFDMC calculation, with the local chiral potential described in the text, at saturation and twice saturation density for the fully spin polarized system. Order by order estimate of the theoretical uncertainties ad LO (red), NLO (green) and $N^2$LO (blue) are provided. Statistical uncertainties from AFDMC are smaller than the size of the points.

from chiral potentials is in reasonable agreement with the one obtained by Krüger at al. [27], at least up to saturation density. For as concerns the EoS derived using the AV8'+UIX interaction, our results are in very good agreement with those obtained in previous work with other potentials of the AVX + Urbana family (see e.g. Refs. [28, 29] for Brueckner-Hartree-Fock calculation with AV18+UIX). In our discussion we will only consider the density range $0.5\rho_0 \leq \rho \leq 2\rho_0$. Another interesting feature to be noticed in the comparison is that the spin symmetry energy, given by the difference between

the energy per neutron of the spin polarized and spin unpolarized systems tends to be substantially larger in EOSA than in EOS$\chi$.

The Monte Carlo results are fitted in order to derive the energy density functional to be used in the TDLSDA response function. We recall that in the Local Density (mean field) Approximation, the energy as a function of the density $\rho$ and the spin polarization $\xi$ can be generically written as:

$$E(\rho, \xi) = T_0(\rho, \xi) + \int \epsilon_V(\rho, \xi) \rho d\mathbf{r}. \tag{3}$$

The kinetic energy $T_0$ as been computed using the bare neutron mass. The quantities $\rho$ and $\xi$ are related to the density of particles with spin up $\rho_\uparrow$ and the density of particle with spin down $\rho_\downarrow$ in the following way:

$$\rho = \rho_\uparrow + \rho_\downarrow; \qquad \qquad \xi = \frac{\rho_\uparrow - \rho_\downarrow}{\rho}. \tag{4}$$

We define the function $\epsilon(\rho, \xi)$ using the common assumption of a quadratic dependence on the spin polarization:

$$\epsilon_V(\rho, \xi) = \epsilon_0(\rho) + \xi^2 \left[ \epsilon_1(\rho) - \epsilon_0(\rho) \right], \tag{5}$$

where the functions $\epsilon_i$ are defined as polynomials in the neutron density:

$$\epsilon_i(\rho) = \quad \epsilon_i^0 + a_i \left( \frac{\rho - \rho_0}{\rho_0} \right) + b_i \left( \frac{\rho - \rho_0}{\rho_0} \right)^2 + c_i \left( \frac{\rho - \rho_0}{\rho_0} \right)^3. \tag{6}$$

Such functions will contain the whole information about the interaction, i.e. all the terms that in ordinary LDA theory for Coulombic systems are separately referred to as "direct", "exchange", and "correlation" terms [30]. The index $i = 0, 1$ will indicate the spin unpolarized and polarized neutron matter ($\xi = 0, 1$) respectively. The expression of the energy density functional in integer powers of the density is connected to the presence of some external field (first power) that in this case stabilizes the asymmetric and/or spin polarized matter, a two-body interaction, a three-body interaction, and so on. In this paper we do not consider explicit dependence on the momentum (i.e. derivatives of the density), nor the possibility of having non-integer exponents. As usual, we assume the value of the saturation density to be $\rho_0 = 0.16$ fm$^{-3}$. Despite there is no implicit or explicit expectation of a hierarchical ordering in our expansion of the density functional, the coefficients fitted on the numerical AFDMC results for EOS-A and EOS-$\chi$, reported in Tab. 1, show some prevalence of the first and second order expansion terms (apart for EOS-$\chi_l$ for SPPNM, which has $b_i$ and $c_i$ of the same order).

In our approach the kinetic energy $T_0$ does not include an effective mass. On the other hand different many methods use the effective mass and claim inconsistent results in the response functions and in neutrino mean free paths either using the effective or the bare mass. On one hand we have to remind that response functions are not physical observables and therefore might differ between the two approaches. On the other hand neutrino mean free paths are physical observables and thus should not be incompatible..

| EOSA | | $\epsilon_i^0$ | $a_i$ | $b_i$ | $c_i$ |
|---|---|---|---|---|---|
| (SPPNM) | $i=1$ | 9.411 | 21.997 | 13.032 | 0.262 |
| (PNM) | $i=0$ | -15.97 | -2.689 | 12.435 | 0.521 |
| EOS$\chi$ | | $\epsilon_i^0$ | $a_i$ | $b_i$ | $c_i$ |
| (SPPNM) | $i=1$ | 3.85 | 10.975 | 6.433 | -1.506 |
| (PNM) | $i=0$ | -17.81 | -7.865 | 7.746 | -0.934 |
| EOS$\chi_u$ | | $\epsilon_0$ | $a_i$ | $b_i$ | $c_i$ |
| (SPPNM) | $i=1$ | 13.87 | 29.206 | 14.573 | -1.502 |
| (PNM) | $i=0$ | -16.36 | -5.117 | 9.367 | -0.565 |
| EOS$\chi_l$ | | $\epsilon_i^0$ | $a_i$ | $b_i$ | $c_i$ |
| (SPPNM) | $i=1$ | -6.18 | -7.256 | -1.707 | -1.510 |
| (PNM) | $i=0$ | -19.26 | -10.614 | 6.126 | -1.303 |

Table 1: Coefficient fitting the density functional of Eq. (6) to the EoS computed by means of the AFDMC method. EOSA refers to the EoS from the AV8′+UIX potential, while the EOS$\chi$ are relative to the Hamiltonian with the local N²LO(D2,E1) chiral interaction. The three tables refer to the center, upper limit and lower limit of the uncertainty band respectively.

It is possible to predict the effective mass emerging from the Monte Carlo calculations from the diffusion of a neutron during the simulation. For instance, a quick estimate of the effective mass ratio at saturation density obtained using a potential of the form AV6′ (inclusive of tensor) gives a value $m^* \sim 0.92$ (See Appendix A for details). This result is in agreement with the results obtained from the study of excited states of the system [31]. However, in this approach the equation of state is inclusive of all the correlation effects leading, among the others, to the correction to the kinetic energy accounted by the effective mass itself, even if our convention is to assume the neutron mass equal to the bare mass. To look at the difference between using the bare mass or the effective mass we evaluated response functions and neutrino mean free paths at saturation energy with the effective mass. We assumed a constant effective mass over the density range $\rho_0/4 \leq \rho \leq 2\rho_0$. We refit the constants of the energy-density function of Eq. (5) to our AFDMC calculations to get a new effective potential consistent with the effective mass. While the response in the longitudinal and transverse channel might be different between the two cases, reshuffling contributions from particle holes and collective modes (see Figs. 3-5), the neutrino mean free path results are qualitatively independent on the choice of either the effective mass or the bare mass (see Figs. 6 and 8).

## 3. Time Dependent Local Spin Density Approximation

The density functional of Eq. (3) can be used to describe the density and spin density excitations by means of the Time Dependent Local Spin Density Approximation (TDLSDA). In the spirit of the mean field theory, the solution of the many-body Schroedinger equation for $N$ neutrons in a volume $V$ such that $\rho = N/V$ is assumed to be the product of two Slater determinants, one for the $N_\uparrow$ spin-up neutrons and one for the $N_\downarrow$ spin-down neutrons:

$$\Psi(\mathbf{r}_1 \ldots \mathbf{r}_N) = \det[\phi_i^\uparrow(\mathbf{r}_j)]\det[\phi_i^\downarrow(\mathbf{r}_j)], \tag{7}$$

where the indices $i, j$ run from 1 to $N^\uparrow$ and $N^\downarrow$ respectively. The spin-up and spin-down neutron densities are defined as:

$$\rho_\sigma = \sum_i |\varphi_i^\sigma(\mathbf{r})|^2, \tag{8}$$

where $\sigma = \uparrow(\downarrow)$ stands for spin-up and spin-down neutrons, respectively, and the sum runs over all the occupied states. By minimizing the energy functional of Eq. (3) with respect to the single particle wavefunction $\varphi_i^\sigma$, one obtains the set of self-consistent, stationary Kohn-Sham equations for spin-up and spin-down neutrons wave functions ($\hbar = c = 1$ hereafter):

$$\left[-\frac{1}{2m}\nabla_\mathbf{r}^2 + v(\rho(\mathbf{r}), \xi(\mathbf{r})) + w(\rho(\mathbf{r})), \xi(\mathbf{r}))\sigma_z + \frac{1}{2}\omega_c\sigma_z\right]\varphi_i^\sigma(\mathbf{r}) = \epsilon_{i,\sigma}\varphi_i^\sigma(\mathbf{r}). \tag{9}$$

The term containing $\omega_c$ is needed to induce a partial (or total) magnetization of neutrons, mimicking the presence of an external (magnetic) field. The value of $\omega_c$ is related to the desired asymmetry $\bar{\xi}$ of the system by requiring that the variation of the expectation energy with respect to $\xi$ at $\bar{\xi}$ be zero [11, 32]. The result of the minimization yields:

$$\omega_c = \bar{\xi}\,\frac{1 + \frac{3}{2\epsilon_F}\left.\frac{\partial w}{\partial \xi}\right|_{\bar{\xi}}}{\frac{3N}{4\epsilon_F}}, \tag{10}$$

where $\epsilon_F = k_F^2/2m$ is the Fermi energy, with the Fermi momentum $k_F$ and the spin-up and spin-down neutron momenta given by $k_F^\uparrow = k_F(1 + \xi)^{1/3}$ and $k_F^\downarrow = k_F(1 - \xi)^{1/3}$, respectively. The effective potentials are defined as the derivatives of the functional with respect to the total density and the magnetization:

$$v(\mathbf{r}) = \frac{\partial \rho\epsilon_V[\rho(\mathbf{r}), \xi]}{\partial \rho(\mathbf{r})}, \quad w(\mathbf{r}) = \frac{\partial \epsilon_V[\rho(\mathbf{r}), \xi]}{\partial \xi(\mathbf{r})}. \tag{11}$$

We will briefly review the derivation of the TDLSDA in the longitudinal and in the transverse channels.

### 3.1. Longitudinal channel

The longitudinal channel describes the response to a time-dependent field along the **r** direction:

$$F^z = \sum_{k=1}^{N} f(\mathbf{r}_k) \lambda_\sigma^k, \tag{12}$$

where:

$$f(\mathbf{r}) = \exp\left[i(\mathbf{q} \cdot \mathbf{r} - \omega t)\right] + \exp\left[-i(\mathbf{q} \cdot \mathbf{r} - \omega t)\right],$$

and $\lambda_\sigma^k = \lambda$ for a *density excitation* and $\lambda_\sigma^k = \lambda \eta_\sigma$, $\eta_\sigma$ is the eigenvalue of the $\sigma_z$ operator ($\eta = 1$ for spin-up and $\eta = -1$ for spin down neutrons) for *vector-density excitations*, $q$ is the momentum and $\omega$ is the energy. The corresponding time dependent Kohn-Sham equations reads:

$$i\frac{\partial}{\partial t}\varphi_i^\sigma(\mathbf{r}, \mathbf{t}) = \left\{-\frac{1}{2m}\nabla_\mathbf{r}^2 + v\left[\rho_\uparrow(\mathbf{r}, t), \rho_\downarrow(\mathbf{r}, t)\right] + w\left[\rho_\uparrow(\mathbf{r}, t), \rho_\downarrow(\mathbf{r}, t)\right]\eta_\sigma \right.$$
$$\left. + \lambda_\sigma\left[e^{i(\mathbf{q}\cdot\mathbf{r}-\omega t)} + e^{-i(\mathbf{q}\cdot\mathbf{r}-\omega t)}\right]\right\}\varphi_i^\sigma(\mathbf{r}, t). \tag{13}$$

For this case we use $\omega_c = 0$, since longitudinal excitations are not directly coupled to the neutron spin. The solutions linearized in the neutron density oscillations induced by external fields are given by:

$$\begin{aligned}\rho_\uparrow(\mathbf{r}, t) &= \rho_\uparrow + \delta\rho_\uparrow(\mathbf{r}, t), \\ \rho_\downarrow(\mathbf{r}, t) &= \rho_\downarrow + \delta\rho_\downarrow(\mathbf{r}, t),\end{aligned} \tag{14}$$

where the time dependent density is assumed to be proportional to the external perturbation:

$$\begin{aligned}\delta\rho_\uparrow(\mathbf{r}, t) &= \delta\rho_\uparrow(e^{i(\mathbf{q}\cdot\mathbf{r}-\omega t)} + e^{-i(\mathbf{q}\cdot\mathbf{r}-\omega t)}), \\ \delta\rho_\downarrow(\mathbf{r}, t) &= \delta\rho_\downarrow(e^{i(\mathbf{q}\cdot\mathbf{r}-\omega t)} + e^{-i(\mathbf{q}\cdot\mathbf{r}-\omega t)}).\end{aligned} \tag{15}$$

Following the derivation in Ref. [10], the density-density response (per unit volume) is then given by:

$$\frac{\chi^s(q, \omega)}{V} = \frac{(\delta\rho_\uparrow + \delta\rho_\downarrow)}{\lambda} \equiv \chi^\uparrow(q, \omega) + \chi^\downarrow(q, \omega), \tag{16}$$

and the vector density-vector density response is:

$$\frac{\chi^v(q, \omega)}{V} = \frac{(\delta\rho_\uparrow - \delta\rho_\downarrow)}{\lambda} \equiv \chi^\uparrow(q, \omega) - \chi^\downarrow(q, \omega). \tag{17}$$

In order to determine the expression of the response function, we can explicitly compute the total self-consistent potentials in the Kohn-Sham equations. At first order in $\delta\rho_\sigma$ this is given by:

$$V_{KS}\left[\rho_\uparrow(\mathbf{r}, t), \rho_\downarrow(\mathbf{r}, t)\right] \equiv v[\rho_\uparrow, \rho_\downarrow] + w[\rho_\uparrow, \rho_\downarrow] =$$
$$= V_{KS}(\rho_\uparrow, \rho_\downarrow) + \left.\frac{\partial V_{KS}}{\partial \rho(\mathbf{r}, t)}\right|_{\rho_\uparrow, \rho_\downarrow}\delta\rho_\uparrow(\mathbf{r}, t) + \left.\frac{\partial V_{KS}}{\partial \rho(\mathbf{r}, t)}\right|_{\rho_\uparrow, \rho_\downarrow}\delta\rho_\downarrow(\mathbf{r}, t), \tag{18}$$

which gives the following expression for the Kohn-Sham equations:

$$i\frac{\partial}{\partial t}\varphi_i^\uparrow(\mathbf{r},t) = \left\{ -\frac{1}{2m}\nabla_\mathbf{r}^2 + \text{const.} + [\delta\rho_\uparrow V_{\uparrow,\uparrow} + \delta\rho_\downarrow V_{\uparrow,\downarrow} + \lambda] \right.$$
$$\left. \times (e^{i(\mathbf{q}\cdot\mathbf{r}-\omega t)} + e^{-i(\mathbf{q}\cdot\mathbf{r}-\omega t)}) \right\}\varphi_i^\uparrow(\mathbf{r},t),$$

$$(19)$$

$$i\frac{\partial}{\partial t}\varphi_i^\downarrow(\mathbf{r},t) = \left\{ -\frac{1}{2m}\nabla_\mathbf{r}^2 + \text{const.} + [\delta\rho_\uparrow V_{\uparrow,\downarrow} + \delta\rho_\downarrow V_{\uparrow,\uparrow} \pm \lambda] \right.$$
$$\left. \times (e^{i(\mathbf{q}\cdot\mathbf{r}-\omega t)} + e^{-i(\mathbf{q}\cdot\mathbf{r}-\omega t)}) \right\}\varphi_i^\downarrow(\mathbf{r},t),$$

where the constant term is the Kohn-Sham potential evaluated at the density and magnetization of the homogeneous neutron matter under consideration. Note that the $\pm$ in the second equation of Eq. (19) comes from the different channels: $+$ for density excitations, while $-$ for vector-density excitations. This fact makes the solutions of the linearized dynamic equations equal to those of the free Fermi gas. As a consequence, the response function of the system will be the one for the free system $\chi_0(q,\omega) = \chi_0^\uparrow(q,\omega) + \chi_0^\downarrow(q,\omega)$, where:

$$\chi_0^\uparrow(q,\omega) = \frac{V\delta\rho_\uparrow}{\lambda_\uparrow'},$$
$$\chi_0^\downarrow(q,\omega) = \frac{V\delta\rho_\downarrow}{\lambda_\downarrow'}.$$

$$(20)$$

The effective strength $\lambda_\sigma'$, defined as:

$$\lambda_\uparrow' = \delta\rho_\uparrow V_{\uparrow,\uparrow} + \delta\rho_\uparrow V_{\uparrow,\downarrow} + \lambda,$$
$$\lambda_\downarrow' = \delta\rho_\uparrow V_{\downarrow,\uparrow} + \delta\rho_\uparrow V_{\downarrow,\downarrow} \pm \lambda$$

$$(21)$$

includes terms depending on the interaction. The mean field potentials $V_{\sigma,\sigma'}$ are obtained through the derivatives of $v + \eta_\sigma w$ with respect to $\rho_\sigma$:

$$V_{\uparrow,\uparrow} = \left.\frac{\partial(v+w)}{\partial\rho_\uparrow(\mathbf{r},t)}\right|_{\rho_\uparrow,\rho_\downarrow} = \left.\left(\frac{\partial}{\partial\rho} + \frac{1}{\rho}\frac{\partial}{\partial\xi}\right)(v+w)\right|_{\rho,\xi},$$
$$V_{\uparrow,\downarrow} = \left.\frac{\partial(v+w)}{\partial\rho_\downarrow(\mathbf{r},t)}\right|_{\rho_\uparrow,\rho_\downarrow} = \left.\left(\frac{\partial}{\partial\rho} - \frac{1}{\rho}\frac{\partial}{\partial\xi}\right)(v+w)\right|_{\rho,\xi},$$
$$V_{\downarrow,\uparrow} = \left.\frac{\partial(v-w)}{\partial\rho_\uparrow(\mathbf{r},t)}\right|_{\rho_\uparrow,\rho_\downarrow} = \left.\left(\frac{\partial}{\partial\rho} + \frac{1}{\rho}\frac{\partial}{\partial\xi}\right)(v-w)\right|_{\rho,\xi},$$
$$V_{\downarrow,\downarrow} = \left.\frac{\partial(v-w)}{\partial\rho_\downarrow(\mathbf{r},t)}\right|_{\rho_\uparrow,\rho_\downarrow} = \left.\left(\frac{\partial}{\partial\rho} - \frac{1}{\rho}\frac{\partial}{\partial\xi}\right)(v-w)\right|_{\rho,\xi}.$$

Comparing Eq. (18) and Eq. (19) we immediately see that:

$$\lambda\chi^\uparrow(q,\omega) = \lambda_\uparrow'\chi_0^\uparrow(q,\omega) = V\delta\rho_\uparrow,$$
$$\lambda\chi^\downarrow(q,\omega) = \lambda_\downarrow'\chi_0^\downarrow(q,\omega) = V\delta\rho_\downarrow.$$

$$(22)$$

The solution of these equations, finally gives the TDLSDA response functions in the longitudinal channel:

$$\chi^s(q,\omega) = V \frac{\chi_0^\uparrow[V-(V_{\downarrow\downarrow}-V_{\uparrow\downarrow})\chi_0^\downarrow] + \chi_0^\downarrow[V-(V_{\uparrow\uparrow}-V_{\downarrow\uparrow})\chi_0^\uparrow]}{(V-V_{\downarrow\downarrow}\chi_0^\downarrow)(V-V_{\uparrow\uparrow}\chi_0^\uparrow) - V_{\uparrow\downarrow}\chi_0^\uparrow V_{\downarrow\uparrow}\chi_0^\downarrow},$$

$$\chi^v(q,\omega) = V \frac{\chi_0^\uparrow[V-(V_{\downarrow\downarrow}+V_{\uparrow\downarrow})\chi_0^\downarrow] + \chi_0^\downarrow[V-(V_{\uparrow\uparrow}+V_{\downarrow\uparrow})\chi_0^\uparrow]}{(V-V_{\downarrow\downarrow}\chi_0^\downarrow)(V-V_{\uparrow\uparrow}\chi_0^\uparrow) - V_{\uparrow\downarrow}\chi_0^\uparrow V_{\downarrow\uparrow}\chi_0^\downarrow}. \tag{23}$$

We should keep in mind that the TDLSDA is valid only in the low-$q$, low-$\omega$ limits. For consistency one should use the expressions of the free response functions $\chi_0^\uparrow$ and $\chi_0^\downarrow$ appearing in the previous equations in the same regime. Their explicit form, which holds for $q \to 0$ and $s = \omega/(qv_F)$ fixed, is:

$$\chi_0^{\uparrow,\downarrow}(\mathbf{q},\omega) = -V\nu^{\uparrow,\downarrow}\left[1 + \frac{s}{2(1\pm\xi)^{1/3}}\ln\frac{s-(1\pm\xi)^{1/3}}{s+(1\pm\xi)^{1/3}}\right], \tag{24}$$

where $\uparrow$ ($\downarrow$) reads with $+$ $(-)$, $\nu^{\uparrow,\downarrow} = mk_F^{\uparrow,\downarrow}/(2\pi^2) = mk_F(1\pm\xi)^{1/3}/(2\pi^2)$, $k_F = (3\pi^2\rho)^{1/3}$ and $s = \omega/(qv_F)$. By defining:

$$\Omega^{\uparrow,\downarrow} = \left[1 + \frac{s}{2(1\pm\xi)^{1/3}}\ln\frac{s-(1\pm\xi)^{1/3}}{s+(1\pm\xi)^{1/3}}\right], \tag{25}$$

we can rewrite the density-density and vector-density/vector-density response functions as:

$$\frac{\chi^{s,v}}{Nm/(2k_F^2)} = -3\frac{(1+\xi)^{1/3}\Omega^\uparrow\left[1+(G_\downarrow\mp(\frac{1-\xi}{1+\xi})^{1/6}G_{\uparrow\downarrow})\Omega^\downarrow\right] + (1-\xi)^{1/3}\Omega^\downarrow\left[1+(G_\uparrow\mp(\frac{1+\xi}{1-\xi})^{1/6}G_{\downarrow\uparrow})\Omega^\uparrow\right]}{(1+G_\downarrow\Omega^\downarrow)(1+G_\uparrow\Omega^\uparrow)-G_{\uparrow,\downarrow}^2\Omega^\uparrow\Omega^\downarrow}, \tag{26}$$

where $G_\uparrow = \nu_\uparrow V_{\uparrow,\uparrow}$, $G_\downarrow = \nu_\downarrow V_{\downarrow,\downarrow}$ and $G_{\uparrow\downarrow} = \sqrt{\nu_\uparrow\nu_\downarrow}V_{\uparrow,\downarrow}$. These parameters can be easily recognized to share the same derivation with the $F_0$ Landau parameters, considering the fact that multiple excitation channels are now possible. This is even more evident simplifying Eq. (26) in the fully polarized and unpolarized neutron matter limits. The response functions for the unpolarized system ($\chi_0^\uparrow = \chi_0^\downarrow = \chi_0$) read:

$$\chi^s(q,\omega) = \frac{\chi_0(q,\omega)}{1 - \frac{\partial v}{\partial\rho}\big|_{\rho,\xi=0}\frac{\chi_0(q,\omega)}{V}} \qquad \chi^v(q,\omega) = \frac{\chi_0(q,\omega)}{1 - \frac{1}{\rho}\frac{\partial w}{\partial\xi}\big|_{\rho,\xi=0}\frac{\chi_0(q,\omega)}{V}}, \tag{27}$$

while for the fully polarized system, where $\chi_0^\downarrow = 0$, we obtain:

$$\chi^s(q,\omega) = \chi^v(q,\omega) = \frac{\chi_0^\uparrow(q,\omega)}{1 - V_{\uparrow,\uparrow}\frac{\chi_0^\uparrow(q,\omega)}{V}}, \tag{28}$$

The resulting expressions of Eqs. (27) and (28) are equivalent to those that could be derived by the Landau Fermi liquids theory considering as quasiparticles spin and density elementary excitations (as combinations of $\delta\rho_\uparrow$ and $\delta\rho_\downarrow$).

The imaginary part of Eq. (26) provides the strength of the single particle excitations:

$$S(q,\omega) = -\frac{1}{\pi}\chi^{s,v}(q,\omega). \tag{29}$$

### 3.2. Transverse channel

The derivation of the response function in the transverse channel, first done by Rajagopal [33], and later applied to quantum dots in Refs. [34, 35], is similar to that used in the longitudinal channel. The excitation operator has the same structure as that of Eq. (12), but the constraint now is that $\Delta S_z = \pm 1$, thereby defining:

$$F^{\pm} = \sum_k f(\mathbf{r_k})\sigma_k^{\pm}. \tag{30}$$

In the $\Delta S_z = \pm 1$ channel, given the magnetization $m$ of the system ($\xi = m/\rho$), the static LSDA equations (9) can be rewritten as:

$$\left[ -\frac{1}{2}\nabla_{\mathbf{r}}^2 + \frac{1}{2}\omega_c\sigma_z + v(\mathbf{r}) + \mathcal{W}\mathbf{m}\cdot\sigma \right] \varphi_i^{\sigma}(\mathbf{r}) = \varepsilon_{i,\sigma}\,\varphi_i^{\sigma}(\mathbf{r}) , \tag{31}$$

where $\mathbf{m}$ is the *spin polarization vector*. The interaction/correlation energy only depends on $\rho$ and $|\mathbf{m}|$, i.e. $\epsilon_V = \epsilon_V[\rho, |\mathbf{m}|]$ so that the spin-dependent interaction/correlation potential $w$ in equation (11) can be written as:

$$\mathcal{W}\mathbf{m} = w[\rho, |\mathbf{m}|]\,\mathbf{m}/|\mathbf{m}| , \tag{32}$$

where:

$$w[\rho, |\mathbf{m}|] = \partial\epsilon_V[\rho, |\mathbf{m}|]/\partial|\mathbf{m}| , \tag{33}$$

and $\mathcal{W}[\rho, |\mathbf{m}|] \equiv w[\rho, |\mathbf{m}|]/|\mathbf{m}|$. Defining the spherical components $\pm$ of the vectors $\mathbf{m}$ and $\sigma$, it is possible to express the $z$ component of the magnetization dependent potential as:

$$w\sigma_z \to \mathcal{W}[\rho, |\mathbf{m}|]\,[m_z\sigma_z + 2(m_+\sigma_- + m_-\sigma_+)]. \tag{34}$$

In the static case, the inclusion of the densities $m_+$ and $m_-$ makes no difference since they vanish identically. The situation is different when the system interacts with a time-dependent field that couples to the nucleon spin through the general term:

$$\mathbf{F}\cdot\sigma = F_z\sigma_z + 2(F_+\sigma_- + F_-\sigma_+) . \tag{35}$$

As a consequence, the interaction Hamiltonian causing transverse spin excitations may be written as:

$$H_{\text{int}} \sim \sigma_f^- e^{-\iota\omega t} + \sigma_f^+ e^{\iota\omega t} . \tag{36}$$

$H_{\text{int}}$ causes non-vanishing variations in the magnetization components $\delta m_+$ and $\delta m_-$ which, in turn, generate at first-order perturbation theory a variation in the mean field potential.

Following the steps described in Ref. [12] the TDLSDA response function is given by (once again $V$ is the volume):

$$\chi_t(q,\omega) = \frac{\chi_t^0(q,\omega)}{1 - \frac{2}{V}\mathcal{W}(\rho, m)\chi_t^0(q,\omega)} , \tag{37}$$

where $\chi_t^0(q,\omega)$ is the free transverse linear response. In the $qv_F \ll \epsilon_F$ limit, where $v_F = k_F/m$ is the Fermi velocity, it is given by:

$$\frac{\chi_t^0(q,\omega)}{V} = -\frac{3}{4}\frac{\rho}{\epsilon_F}\left(1 + \frac{\omega}{2qv_F}\ln\frac{\omega - \omega_a - qv_F}{\omega - \omega_a + qv_F}\right), \tag{38}$$

where:

$$\omega_a = \frac{\omega_c}{\left(1 + \frac{3\rho\mathcal{W}(\rho,m)}{2\epsilon_F}\right)} = \frac{2}{3}\frac{k_F^2}{m}\xi ,$$

and the last step has been obtained by using relation (10).

The imaginary part of Eq. (37) provides the excitations strengths $S^\pm(q,\omega) = \sum_n |\langle n|\tau_f^\pm|0\rangle|^2\delta(\omega - \omega_{no})$ corresponding to the $\Delta S_z = \pm 1$ channels, respectively, through the relation:

$$S^-(q,\omega) - S^+(q,-\omega) = -\frac{1}{\pi}\text{Im}(\chi_t) . \tag{39}$$

As we did for Eqs. (24) and (25), Eqs. (37) and (38) can then be recast in the following way using the dimensionless variables $s = \omega/(qv_F)$ and $z = 3q/(2k_F\xi)$:

$$\frac{\chi_t^0(q,\omega)}{V\nu} \equiv \frac{\chi_t^0(s,z)}{V\nu} = \Omega_\pm(s,z), \tag{40}$$

with

$$\nu = mk_F/\pi^2,$$

$$\Omega_\pm(s,z) = -\left(1 + \tfrac{s}{2}\ln\tfrac{s-1-1/z}{s+1-1/z}\right),$$

and

$$\frac{\chi_t(q,\omega)}{V\nu} \equiv \frac{\chi_t(s,z)}{V\nu} = \frac{\Omega_\pm(s,z)}{1 - 2\nu\mathcal{W}(\rho,m)\Omega_\pm(s,z)}. \tag{41}$$

The $\pm$ in the definition in $\Omega$ indicates that it includes both the $\Delta S = +1$ and $\Delta S = -1$ channels.

## 4. Numerical results

### 4.1. Response and excitation strengths

The numerical evaluation of the longitudinal and transverse response functions gives access to information about the neutron dynamics. The single particle excitations strengths are computed using Eqs. (29) and (39). On the other hand, the poles of Eqs. (26) and (41) are the energies of the collective modes of the system. Naming $N(s)$ and $D(s)$ the numerators and the denominators of Eqs. (26) and (41), respectively, we expand around the poles at $s = \bar{s}$ to evaluate the strength as:

$$\frac{S(s)}{V\nu} = \frac{N(s)}{\partial D/\partial s}\delta(s - \bar{s}) , \qquad \text{and} \qquad \frac{S(s)}{Nm/(2k_F^2)} = \frac{N(s)}{\partial D/\partial s}\delta(s - \bar{s}) \tag{42}$$

for the longitudinal and the transverse channel respectively. The collective modes are indicated by arrows in Figs. 3-5. In the longitudinal channel the strength of the collective modes have been rescaled: longer arrows correspond to dominant scalar or vector contribution (their strength would be too small compared to the particle-hole contribution). In the transverse channel the correct strength has been plotted instead.

We report in Fig. 3 the results obtained from the calculation of the longitudinal response functions for the two different potentials used, i.e. the phenomenological AV8′+UIX interaction and the local chiral potential at N²LO. The plots are made as functions of the dimensionless quantity $s = \omega/(qv_F)$ for a fixed value of the spin polarization $\xi = 0.2$, and for three different values of the density which are characteristic of the outer core of a neutron star ($\rho = 0.08, 0.16,$ and $0.32$ fm$^{-3}$).
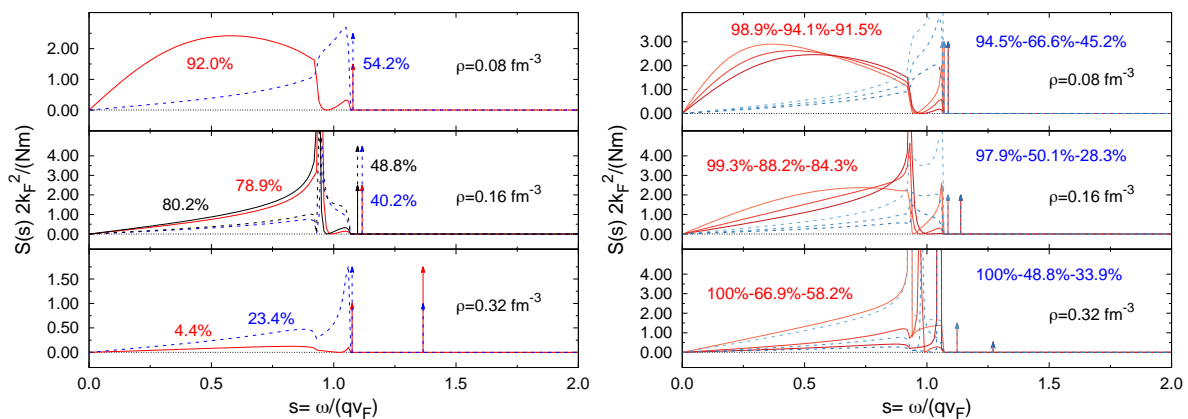


Figure 3: Longitudinal response function at spin polarization $\xi = 0.2$ for AV8′+UIX (left) and chiral potential at N²LO (right). The red solid lines and blue dashed lines stand for density and spin density Dynamical Structure Factors (DSFs) respectively. Arrows indicate the presence of a collective mode. The percentages in the plot show the fraction of the total strength pertinent to the particle-hole excitations. The black lines at saturation density for the phenomenological potential (left) show the results using the effective mass instead of the bare mass. Note that the effective mass enters in the definition of the variable $s$. On the right panel the three lines for each DSF keep track of the theoretical uncertainties obtained using chiral effective interaction. Lighter to darker curves stand for lower-central-higher EOS$_\chi$ of Fig. 1 and Tab. 1. The same color scheme holds for Fig. 4.

In Fig. 4 the same quantity is reported for spin unpolarized neutron matter. The percentages reported in the graphs show the fraction of the total strength relative to the particle-hole contribution. Arrows represent the presence of collective modes (the size is not proportional to the strength). For the response computed using the N²LO potential we propagated the theoretical uncertainty. As expected, at the lowest density considered the results are qualitatively and quantitatively very insensitive to the specific interaction used. At saturation density and above, the theoretical uncertainty on the pressure reflects in a more pronounced difference in the characterization of the single

particle spectrum, in particular for as concerns the scalar channel in the region around $\omega = qv_F$. The vector channel is somewhat less affected, at least qualitatively, by the theoretical uncertainty.
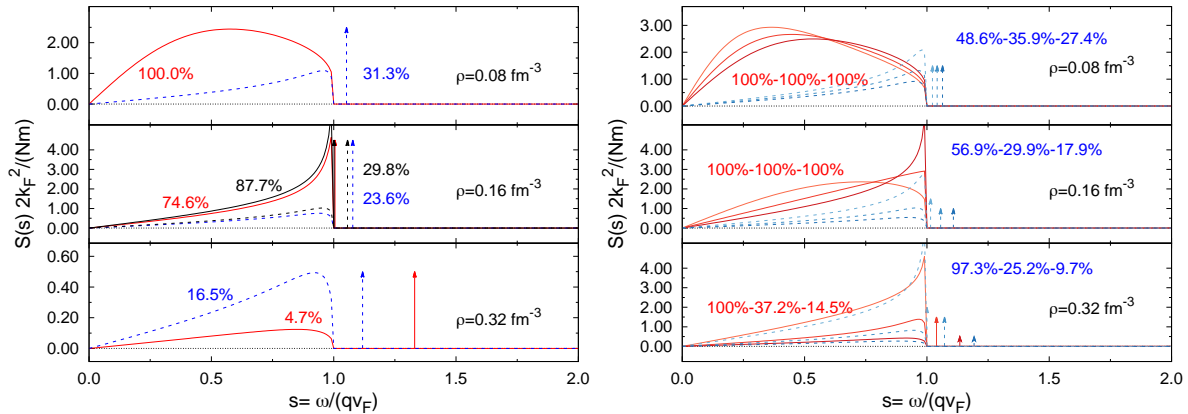


Figure 4: Longitudinal response function for AV8′+UIX (left) and chiral potential at N²LO (right) at spin polarization $\xi = 0.0$, i.e. PNM. The color scheme is described in Fig. 3.

A similar behavior concerns the collective modes. The energy of the collective modes strongly depends on the stiffness of the equation of state. A consequence is that the energy of the collective modes when increasing the density results significantly higher in the AV8′+UIX case. It should be noticed that in pure neutron matter collective modes are not present for the lowest density considered in the scalar channel. On the contrary, the results at $\xi = 0.2$ always show the presence of a collective mode. There is some further systematics to be noticed in the behavior of the collective modes. At $\xi = 0$ the spin mode appears with a dispersion for $q \sim 0$ more or less independent of the density, whose strength is only slightly increasing with $\rho$. This is in contrast with the density mode that begins to have significant strength only at densities around saturation, and quickly increases its dispersion coefficient. This fact points to a substantially different nature of these excitations. In particular the spin mode appears to be similar to a spin-density wave in neutron matter. The polarization of the medium induces a coupling between the spin and the density modes due to the spin imbalance. This translates into the appearance of a low strength density mode at the same energy of the spin one for low densities. At higher densities the two collective excitations separate in energy essentially in the same way as in the $\xi = 0$ case, although the mixing is still visible in the presence of a second, low strength peak for both modes.

For the transverse response, positive values of $s$ describe the excited states in the $\Delta S_z = -1$ channel, while for negative values of $s$ the excited states in the $\Delta S_z = +1$ channel. In Fig. 5 we show the results for the transverse response function. In this case, instead of fixing the polarization we fixed the value $z = 3q/(2k_F\xi) = 6$, still corresponding to a case of low magnetization. The results are qualitatively very close to those obtained for the longitudinal channel, although the dependence on the specific

choice of the interaction results weaker, both for the particle-hole and the collective part of the spectrum. Contrary to what happens in the longitudinal channel, both collective modes do not show a significant variation of the linear dispersion coefficient with the density. It is interesting to observe, however, that the coefficient is very different between the $\Delta S_z = -1$ and the $\Delta S_z = 1$ excitations. This means that the two modes have a gap that is proportional to the neutron matter polarization.
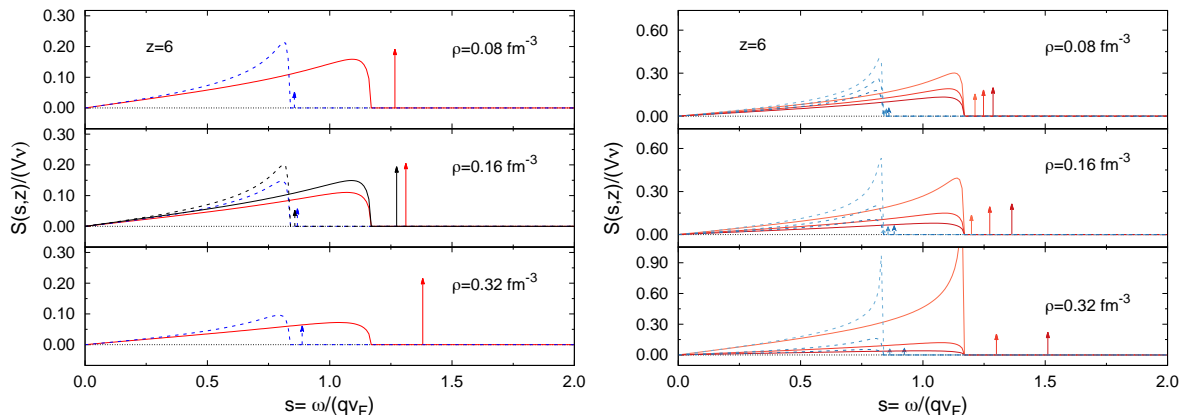


Figure 5: Transverse response function at low spin polarization ($z = 6$) for AV8'+UIX (left) and for chiral potential at N$^2$LO (right). Recall that $z = \frac{3q}{2k_F\xi}$, so $z > 1$ means small $\xi$. The full and dashed lines indicate the particle/hole and collective strengths in the $\Delta S_z = -1$ ($s > 0$ - red) and $\Delta S_z = +1$ ($s < 0$ - blue, which has been plotted flipped and in the $s > 0$ region) channels respectively. The black lines at saturation density for the phenomenological potential (left) show the results using the effective mass instead of the bare mass. Note that the effective mass enters in the definition of the variable $s$. On the right panel the three lines for each DSF keep track of the theoretical uncertainties obtained using chiral effective interaction. Lighter to darker curves stand for lower-central-higher EOS$_\chi$ of Fig. 1 and Tab. 1.

### 4.2. Neutrino mean free path

The neutrino processes considered are the neutral-current scattering $n + \nu \to n + \nu$, neutron bremsstrahlung $n + n \to n + n + \nu + \bar{\nu}$ and its inverse $n + n + \nu + \bar{\nu} \to n + n$. Also the inelastic scattering process $\nu + n + n \to n + n + \nu$ is included [36]. Note that we are working with PNM, so we are not considering $\beta$-decay processes or any other process involving protons. The neutrino mean free path (NMFP) can be computed by integrating the total excitation strength $S(q, \omega)$ (in both the longitudinal and transverse channels), to first obtain the total neutrino cross section $\sigma$ [37, 38]:

$$\sigma = \frac{G_F^2}{2} \frac{1}{E} \int dq \int d\omega (E - \omega) q \left[ 1 + \frac{E^2 + (E - \omega)^2 - q^2}{2E(E - \omega)} \right] S(q, \omega), \qquad (43)$$

where $E$ is the incident neutrino energy, and $G_F = 1.166 \times 10^{-5}$ GeV$^{-2}$. Integration must be performed on a region of $q$ and $\omega$ compatible with the scattering, as discussed

for instance in Ref. [37]. We will assume neutrinos to be ultra-relativistic and non-degenerate. The NMFP $\lambda$ can be derived from the total neutrino cross section $\sigma$ from the relation $\lambda = 1/(\sigma\rho)$.

From existing estimates of neutron spin susceptibility [39], we expect the induced spin polarization to be low even in presence of strong magnetic fields. We could estimate the order of magnitude of the spin polarization as

$$2m\Delta E = \mu_n B \ , \tag{44}$$

where $m$ is the neutron mass, $\mu_n$ is the Bohr magneton and $B$ is the magnetic external field. $\Delta E$ is the energy difference between the fully spin polarized and the spin unpolarized system. The maximum superficial magnetic field observed for a magnetar is $B_{\mathrm{surf}} \sim 10^{10} - 10^{11}$ T. This would lead to an expected spin polarization of the order of $10^{-5} - 10^{-4}$ at saturation density. Internal dynamo effects might power up the magnetic field by a factor $10^2 - 10^3$, which leads to an expected spin polarization $\xi \sim 10^{-3} - 10^{-1}$.

In Fig. 6 we report the results we obtained at saturation density for spin polarization $\xi = 0.0$ and $\xi = 0.1$ and compared them with the result obtained for PNM with a more refined method [40] using the correlated Tamm-Dancoff approximation (CTDA). Within the CTDA [38] the states are expressed as a basis of correlated 1p-1h excitations. The correlations are then encoded in effective operators acting on 1p-1h states. The NMFP for spin unpolarized pure neutron matter is essentially independent of the incident energy of the neutrinos. The presence of a small spin-asymmetry shows instead non trivial patterns, significantly increasing the neutron matter opacity for low neutrino energies.

The estimated theoretical uncertainty on the results computed from the chiral interaction are quite significant. Nevertheless, the prediction obtained making use of the phenomenological interaction differ by about 20% from that of the N²LO potential (central value), and it is close to the upper limit predicted by the propagated uncertainty.

In Fig. 7 we compare our results for the NMFP ratio at saturation density to those of Pastore et al. [4] and to those of Lovato et al. [40]. The first paper presents computations using a Skyrme force explicitly including tensor contributions, which we instead do not address with specific terms. The second case also includes explicit correlations introduced via the Tamm-Dancoff approximation. All results tend to overlap in a region around $\lambda/\lambda_{FG} \sim 2$. Skyrme results, however, tend to predict a lower value of NMFP. This might be due to the different treatment of correlations. A similar effect is also visible in the comparison of the Tamm-Dancoff results and our results for the Argonne potential. It should be remarked, however, that all these results start from different neutron-neutron interaction schemes, and it is overly difficult to attribute in a clear way the differences either to the potential used or to the degree of approximation of the functional employed.

In Fig. 8 we show the contribution of the different channels to the total neutrino mean free path. As an example we report the results for the phenomenological potential AV8'+UIX at spin polarization $\xi = 0.1$.
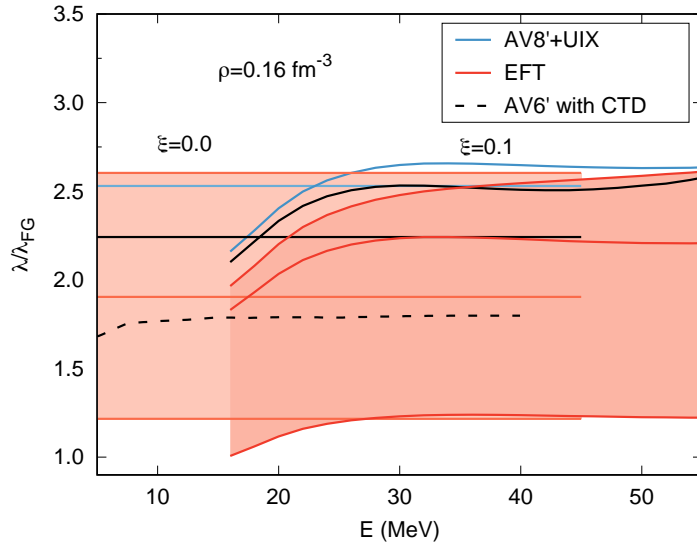
Figure 6: Neutrino mean free path ratio with respect to the free Fermi gas at saturation density $\rho_0 = 0.16$ fm$^{-3}$ for spin polarization $\xi = 0.1$ and for PNM ($\xi = 0$). Top-middle-bottom lines for EFT refer to higher-central-lower EOS$_\chi$ of Fig. 1 and Tab. 1. The results for the phenomenological potential with the effective mass are plotted in black full lines. Black dashed lines show the results of Lovato et al. [40] (black solid lines) with AV6' using the correlated Tamm-Dancoff (CTD) approximation.
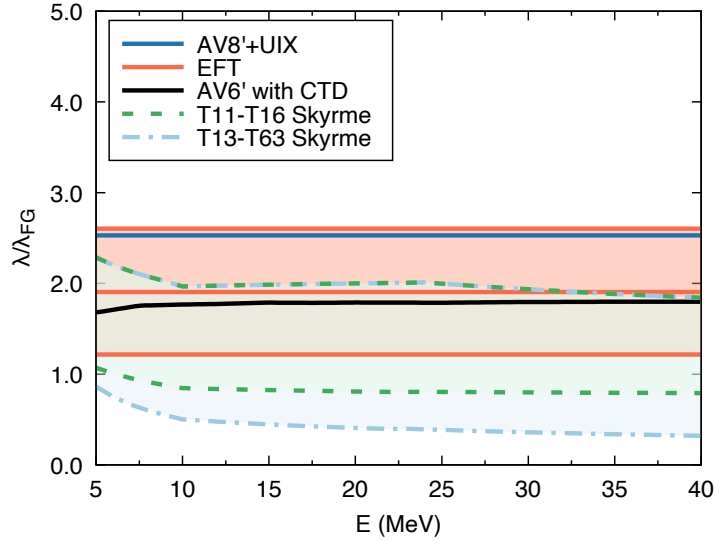


Figure 7: NMFP for PNM at saturation density from the present work compared to those obtained by Lovato et al. [40] (black solid lines) and by Pastore et al. [4] (dashed and dash-dotted lines). In the latter case different bands correspond to different choices of the tensor term of the Skyrme potential. Top-middle-bottom lines for EFT refer to higher-central-lower EOS$_\chi$ of Fig. 1 and Tab. 1.
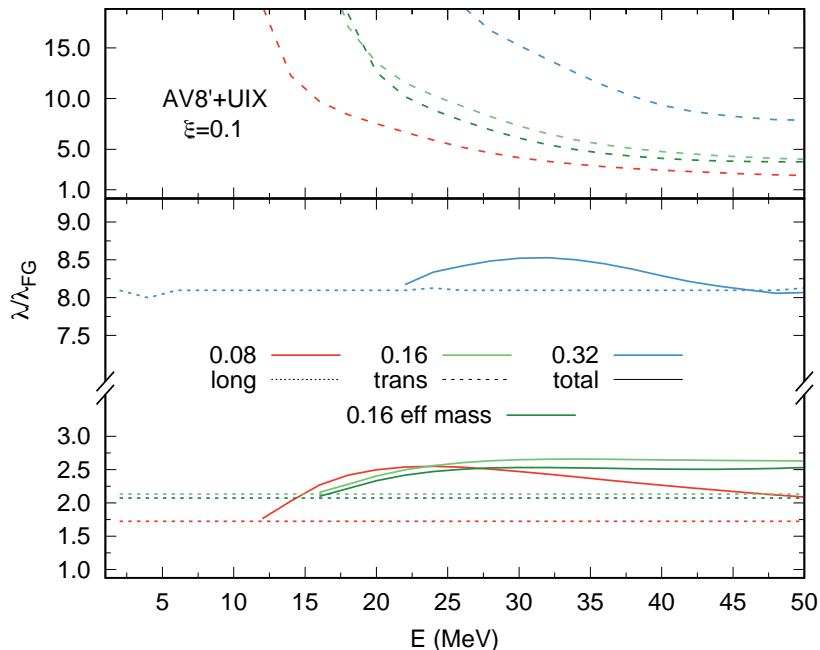
Figure 8: Neutrino mean free path ratio with respect to the free FG for spin polarization $\xi = 0.1$ as a function of density. Dotted lines are the contributions coming from the longitudinal channels, dashed lines from the transverse part, while solid lines show the total mean free path. The contribution using for the effective mass are in dark green.

Results are plotted at saturation density $\rho_0 = 0.16$ fm$^{-3}$, half and twice saturation density. We observe that at all densities the contribution coming from the longitudinal part is almost constant as a function of the energy of the incident neutrino. We observe that for both channels NMFP increases with the density. However, since the relative weight of the two contributions is different for each densities the result gives a total NMFP with non-trivial density dependence.

To understand the implication of spin-polarization to the NMFP we show in Fig. 9 the NMFP in function of the energy of the incident neutrino. The NMFP has to be compared to the radius of the neutron star ($\approx 1.2 - 1.5 \cdot 10^4$ m): above this value matter is essentially transparent to neutrinos, while the typical energies of the neutrinos of astrophysical interest are in the range $0.1 - 50$ MeV [41, 42].

## 4.3. Compressibility

In order to make an even more direct comparison between our approach and other microscopical models, useful to assess its validity, we will discuss here the compressibility of PNM, a parameter that directly influences NMFP and other properties of astrophysical interest, in particular the structure of neutron stars.

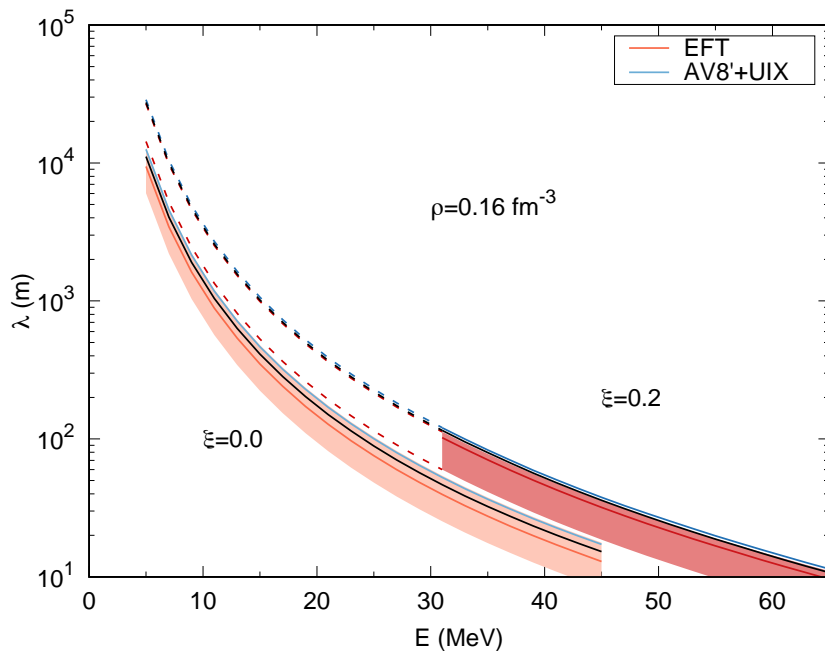Given a fit of the equation of state as the one in Eq. (5), it is possible to directly

Figure 9: Neutrino mean free path for PNM and for spin polarization $\xi = 0.2$ as a function of incident neutrino energy. In PNM the longitudinal and transverse channel contribute equally to the total NMFP, while as soon as there is some spin polarization we can observe an energy threshold under which the NMFP is entirely determined by the longitudinal response (dashed lines). The same behavior can be seen also in Fig. 8 at various densities. Top-middle-bottom lines for EFT refer to higher-central-lower $\mathrm{EOS}_\chi$ of Fig. 1 and Tab. 1. The results for the phenomenological potential with effective mass are plotted in black.

extract the compressibility from the definition:

$$K = -\frac{1}{V}\frac{\partial V}{\partial P}, \tag{45}$$

by rewriting it as a function of the energy per nucleon:

$$\frac{1}{K} = \rho^2 \left( \rho \frac{\partial^2 E/N}{\partial \rho^2} + 2 \frac{\partial E/N}{\partial \rho} \right). \tag{46}$$

However, the quantity that is usually reported is the compression modulus or incompressibility, which is defined as:

$$K_\infty = k_F^2 \frac{d^2 E/A}{dk_F^2}, \tag{47}$$

The two quantities are directly related by the following expression:

$$K_\infty = \frac{9}{\rho}\frac{1}{K}. \tag{48}$$

In this case we can check the consistency of our results using two independent ways to estimate the compressibility of PNM: 1) starting from the energy-density function using equation (46), and 2) using the inverse energy weighted sum rule $m_{-1}$. As an example, in the scalar and vector longitudinal channels, $m_{-1}$ reads [10]:

$$m_{-1}^{s,v} = \frac{V}{2} \frac{\nu_\uparrow(1 + G_\downarrow) + \nu_\downarrow(1 + G_\uparrow) \mp 2\sqrt{\nu_\downarrow \nu_\uparrow} G_{\uparrow\downarrow}}{(1 + G_\downarrow)(1 + G_\uparrow) - G_{\uparrow\downarrow}^2}, \qquad (49)$$

where the minus sign is for the scalar case, while the plus sign holds for the vector case. In the case of spin-unpolarized PNM ($\xi = 0.0$) we have that $\nu_\uparrow = \nu_\downarrow = \nu$ and $G_\uparrow = G_\downarrow = G$ and we can write:

$$\frac{m_{-1}^s}{m_{-1}^0} = \frac{K}{K_0} = \frac{1}{1 + G + G_{\uparrow\downarrow}^2}, \qquad (50)$$

where $m_{-1}^0 = V\nu/2$ and $K_0 = 9\pi^2 m/k_F^5$ respectively are the Fermi gas static polarizability and compressibility. The values we estimate within our approach using the two methods are always numerically indistinguishable.

Eq. (50) shows once more the relationship between this approach and the Landau theory. The parameter $G$ can in principle be identified with $F_0$. This means, however, that the TDLSDA estimate of the compressibility also includes an order $G^2$ correction.
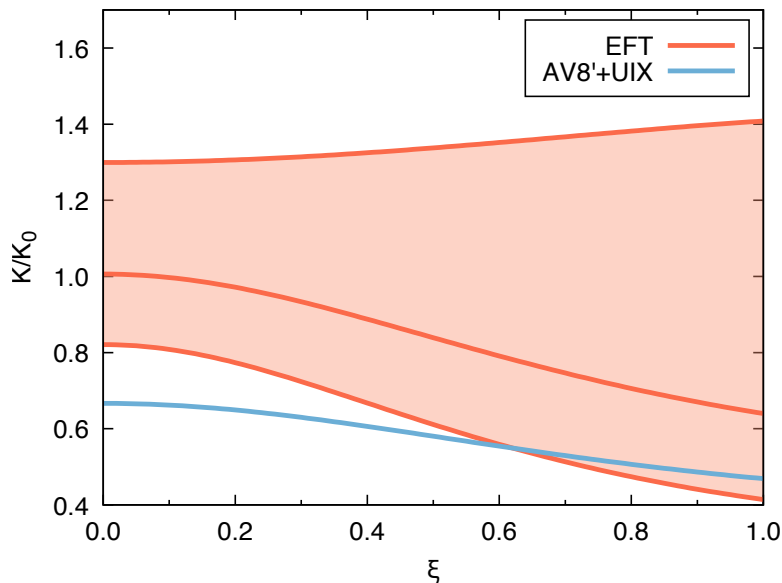


Figure 10: Compressibility ratio for PNM at saturation density as a function of the spin asymmetry. Top-middle-bottom lines for EFT refer to lower-central-higher EOS$_\chi$ of Fig. 1 and Tab. 1.

The compressibility computed at saturation density as a function of the spin asymmetry $\xi$ for the two different potentials used in this work is shown in Fig. 10.

Interestingly enough, the chiral EFT potential would predict a compressibility ratio decreasing with $\xi$. However, at the lower limit of the predicted theoretical errorbar this behavior is inverted. In this case the Argonne-Urbana potential gives a substantially different value at $\xi = 0$, but tends to close the gap with the EFT potential for the fully spin polarized case. In Fig. 11 we show the compressibility ratio as a function of the density for the spin unpolarized PNM. As expected, the compressibility decreases as a
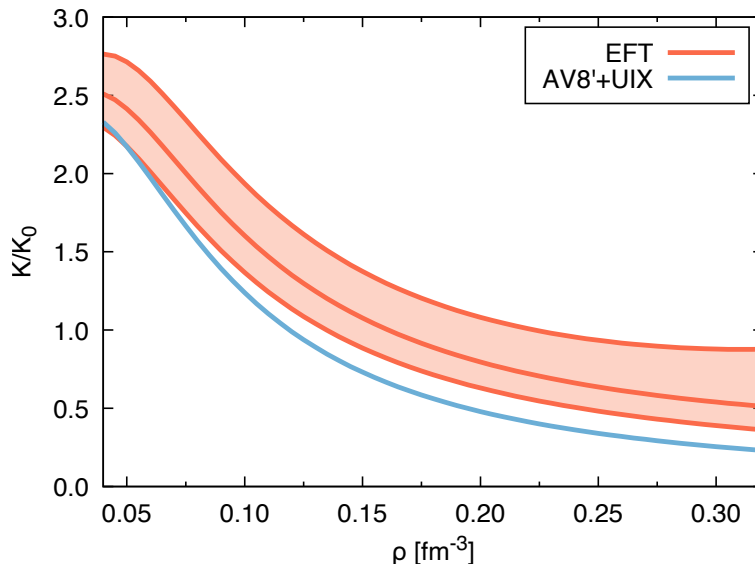


Figure 11: Compressibility ratio for spin unpolarized PNM in function of the density. Top-middle-bottom lines for EFT refer to lower-central-higher EOS$_\chi$ of Fig. 1 and Tab. 1.

function of the density. Chiral EFT potential systematically yields an higher value as a direct consequence of the fact the EoS for PNM is softer than the one obtained using the phenomenological AV8′+UIX potential.

We report in Table 2 a comparison of our prediction for the compressibility and the compression modulus to other results available in literature. Also in this case our approach tends to emphasize the effects of the stiffness of the EoS with respect to other methods. In particular it is interesting to compare the values obtained by the Correlated Basis Function (CBF) calculations of Benhar et al. [44], employing a two-body interaction only, to our results obtained with the Argonne-Urbana potential. The latter are higher of about a factor 2. However, this discrepancy is substantially reduced when comparing to the Fermi Hyper-Netted Chain (FHNC) results of Akmal and Pandharipande [46], essentially employing the same potential. Results obtained with chiral EFT tend instead to be closer to the other values reported in literature, and in particular to the results coming from HF or Brueckner-HF calculations. All these discrepancies point to the fact that a more systematic and homogeneous comparison between different approaches is definitely in order.

| $\rho = 0.032$ fm$^{-3}$ | K/K$_0$ | K/$\hbar c$ [fm$^4$] |
|---|---|---|
| AV8$'$+UIX | 2.38 | 1103 |
| EFT | 2.51 | 1162 |
| BHF [43] | 2.54 | 1176 |
| Skyrme [43] | 2.57 | 1191 |
| QHD [43] | 3.17 | 1467 |
| $\rho = 0.16$ fm$^{-3}$ | K/K$_0$ | $(\hbar c)^2 \cdot$K$_\infty$ [MeV] |
| AV8$'$+UIX | 0.67 | 526.1 |
| EFT | 1.01 | 348.6 |
| AV18 (CBF) [44] | 1.08 | 324.7 |
| BKR $\rho < 0.182$ fm$^{-3}$ [45] | 2.83 | 123.8 |
| BKR $\rho > 0.182$ fm$^{-3}$ [45] | 1.09 | 320.8 |
| $\rho = 0.20$ fm$^{-3}$ | K/K$_0$ | $(\hbar c)^2 \cdot$K$_\infty$ [MeV] |
| AV8$'$+UIX | 0.48 | 849.3 |
| EFT | 0.80 | 511.3 |
| AV18+UIX (FHNC) [44, 46] | 0.69 | 589.8 |
| AV18 (CBF) [44] | 0.88 | 462.4 |

Table 2: Compressibility in PNM. The results of this work are denoted as AV8$'$+UIX and EFT for the Argonne-Urbana and chiral EFT interactions respectively. BKR are the results obtained fitting Brueckner-HF calculations employing the Bressel-Kerman-Rouben potential, as reported by J.W. Clark et al. in Ref. [45]. AV18 (CBF) are the Correlated Basis Functions of Benhar et al. from Ref. [44]. AV18+UIX (FHNC) are the Fermi Hyper-Netted Chain of Akmal and Pandharipande [46]. BHF, Skyrme and QHD are Brueckner-Hartree-Fock, Skyrme force based Hartee-Fock (HF) and Quantum Hydrodynamical calculations respectively as reported in the paper from Aguirre et al. in Ref. [43].

## 5. Conclusions

We successfully extended TDLDA to study the response function of neutron matter with arbitrary spin polarization both in the longitudinal and in the transverse channel starting from accurate QMC calculations of the equation of state for PNM and for SPPNM. We employed two different neutron-neutron potentials, the phenomenological AV8$'$+UIX and a modern local chiral EFT potential. For the latter, we considered the predicted theoretical uncertainties coming from the expansion scheme of the theory. We computed estimates for the NMFP showing non trivial contribution coming from the two different channels and also the effects of a small spin polarization, which could play a role in high energy phenomena such as neutron star mergers and supernova explosions. At the neutron core conditions matter is essentially transparent to neutrinos, while relevant effects could be seen in the neutron star crust.

## Appendix A. Calculation of the effective mass

The effective mass ratio can be directly estimated from the self-diffusion coefficient of a particle in a DMC calculation. We present the results obtained for a system of 14 neutrons in which periodic boundary conditions have been turned off. The diffusion coefficient was computed for the FG and for an interacting system of neutrons interacting with the two-body AV6′ potential, which includes the tensor term, at saturation density. First we computed the averaged squared distance $\langle r^2 \rangle$ travelled by a neutron in a random walk as a function of the diffusion time as shown in Fig. A1. This quantity is strictly related to the kinetic part of the imaginary time propagator:

$$
\begin{aligned}
G_0(R', R) &= \langle R'|e^{-T\delta\tau}|R\rangle. \\
&= \left(\frac{m}{2\pi\hbar^2\delta\tau}\right)^{\frac{3N}{2}} e^{-\frac{m(R-R')^2}{2\hbar^2\delta\tau}} \ ,
\end{aligned}
\tag{A.1}
$$

which is formally equivalent to the Green's function of a diffusion equation in which the diffusion constant $\widetilde{D} \propto \hbar^2(m_n/\widetilde{m})$, where $m_n$ is the bare neutron mass. To estimate the effective mass ratio $m^*$ one just needs to compute the ratios:

$$
m^* = \frac{\widetilde{m}}{m} = \frac{D}{\widetilde{D}} \ ,
\tag{A.2}
$$

where $D$ and $m$ are the diffusion coefficient and the mass respectively in the case of the FG.

In order to estimate $D$ and $\widetilde{D}$, we performed two fits on two different time windows on each data set to check the accuracy of our fit. The first fit has been performed in the time interval $(0.1 - 0.3)$ fm$^{-1}$ and the other in the range $(0.1 - 0.2)$ fm$^{-1}$. The two fits give essentially the same effective mass ratios ($m_1^* = 0.918$ and $m_2^* = 0.923$). In Fig. A1 we plot the fit relative to the larger time interval only. Comparing our result to the one obtained with the calculation of the effective mass ratio derived from non-perturbative calculations of the single-particle excitation spectrum of Ref. [31] we see a good agreement even if we only employed the two-body potential AV6′ rather than the full two- plus three-body interaction AV8′+UIX.
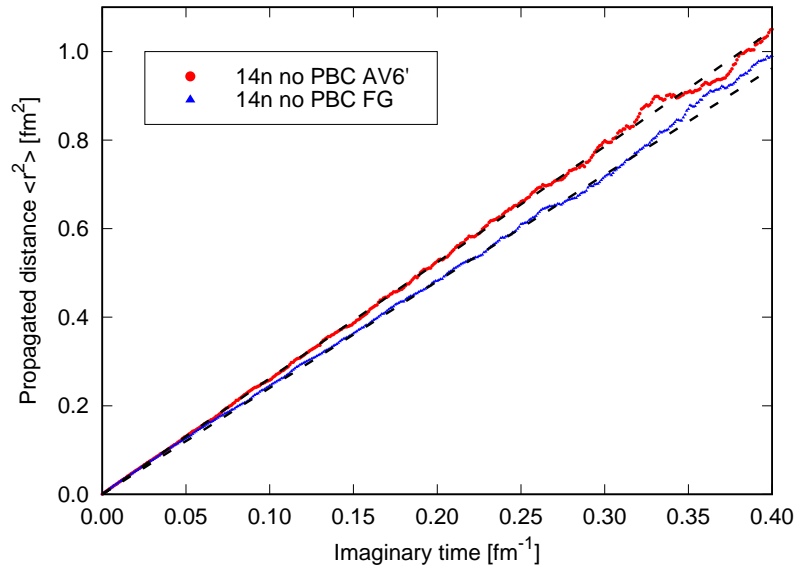
Figure A1: Calculation of the diffusion coefficient for the case of the FG and for a system interacting with the two-body potential AV6′ at saturation density $\rho_0 = 0.16 \, \text{fm}^{-3}$. The dashed line represents the fit to the two data-sets (see text for details).

# References

[1] Weinberg S 1972 Phys. Rev. D **5** 1412

[2] Sawyer R F 1975 Phys. Rev. D **11** 2740

[3] Burrows A and Sawyer R F 1998 Phys. Rev. C **58** 554

[4] Pastore A, Martini M, Buridon V, Davesne D, Bennaceur K and Meyer J 2012 Phys. Rev. C **86** 044308

[5] Pastore A, Martini M, Davesne D, Navarro J, Goriely S and Chamel N 2014 Phys. Rev. C **90** 025804

[6] Pastore A, Davesne D and Navarro J 2015 Phys. Rep. **563**

[7] Cowell S and Pandharipande V R 2003 Phys. Rev. C **67** 035504

[8] Benhar O and Valli M 2007 Phys. Rev. Lett. **99** 232501

[9] Lovato A, Losa C and Benhar O 2013 Nuc. Phys. A **901** 22

[10] Lipparini E and Pederiva F 2013 Phys. Rev. C**88** 024318

[11] Lipparini E *Modern Many-Particle Physics* (World Scientific, Singapore 2003)

[12] Lipparini E and Pederiva F 2016 Phys. Rev. C**94** 024323

[13] Gezerlis A, Tews I, Epelbaum E, Gandolfi S, Hebeler K, Nogga A and Schwenk A 2013 Phys. Rev. Lett. **111** 032501

[14] Gezerlis A, Tews I, Epelbaum E, Freunek M, Gandolfi S, Hebeler K, Nogga A and Schwenk A 2014 Phys. Rev. C **90** 054323

[15] Lynn J E, Tews I, Carlson J, Gandolfi S, Gezerlis A, Schmidt K E and Schwenk A 2016 Phys. Rev. Lett. **116** 062501

[16] Tews I, Gandolfi S, Gezerlis A and Schwenk A 2016 Phys. Rev. C **93** 024305

[17] Tews I, Carlson J, Gandolfi S and Reddy S 2018 Astrophys. J. **860** 149

[18] Schmidt K E and Fantoni S 1999 Phys. Lett. B **446** 99

[19] Gandolfi S, Illarionov A Y, Schmidt K E, Pederiva F and Fantoni S 2009 Phys. Rev. C **79** 054005

[20] Gandolfi S, Gezerlis A and Carlson J 2015 Annu. Rev. Nucl. Part. Sci. **65:1** 303

[21] Carlson J, Gandolfi S, Pederiva F, Pieper S C, Schiavilla R, Schmidt K E and Wiringa R B 2015

Rev. Mod. Phys. **87** 1067

[22] Gandolfi S, Carlson J, Reddy S, Steiner A W and Wiringa R B 2014 Eur. Phys. J. A **50** 10

[23] Ceperley D M, Alder B J, 1980 Phys. Rev. Lett. **45** 566

[24] Zong F H, Ceperley D M, Moroni S, Fantoni S 2003 Mol. Phys **101** 1705

[25] Epelbaum E, Krebs H and Meissner U -G 2015 Eur. Phys. J. A **51** 53

[26] Lonardoni D, Gandolfi S, Lynn J E, Petrie C, Carlson J, Schmidt K E, Schwenk A 2018, Phys. Rev. C **97** 044318

[27] Krüger T, Hebeler K and Schwenk A 2015 Phys. Lett. B **744** 18

[28] Bombaci I, Polls A, Ramos A, Rios A, Vidaña I 2006, Phys. Lett. B **632** 638

[29] Vidaña I, Polls A, Durant V 2016, Phys. Rev. C **94** 054006

[30] Hoenberg P and Kohn W 1964 Phys. Rev. **136** B864

[31] Ismail N, Buraczynski M and Gezerlis A 2019 Phys. Rev. Lett. **122** 152701

[32] Lipparini E, Colletti L, Orlandini G and Serra L 1998 Cz. J. of Phys. **48** 725

[33] Rajagopal A K 1978 Phys. Rev. B **17** 2980

[34] Lipparini E and SerraL 1998 Phys. Rev. B **57** R6830

[35] Lipparini E, Barranco M, Emperador A, Pi M and Serra Ll 1999 Phys. Rev. B **60** 8734

[36] Hannestad S and Raffelt G 1998 Astrophys. J. **507** 339

[37] Iwamoto N and Pethick C J 1982 Phys. Rev. D **25** 313

[38] Cowell S and Pandharipande V R 2004 Phys. Rev. C **70** 035801

[39] Fantoni S, Sarsa A and Schmidt K E 2001 Phys. Rev. Lett. **87** 181101

[40] Lovato A, Benhar O, Gandolfi S and Losa C 2014 Phys. Rev. C **89** 025804

[41] Reddy S, Prakash M, Lattimer J M and Pons J A 1999 Phys. Rev. C **59** 2888

[42] Ejiri H 2000 Phys. Rep. **338** 265

[43] Aguirre R, Bauer E and Vidaña I 2014 Phys. Rev. C **89** 035809

[44] Benhar O, Cipollone A and Loreti A 2013 Phys. Rev. C **87** 014601

[45] Clark J W, Heintzmann H, Hillebrandt W and Grewing M 1972 Astroph. Lett **10** 21

[46] Akmal A, Pandharipande V R and Ravenhall D G 1998 Phys. Rev. C **58** 1804